ANALYSIS OF MICROBUNCHING STRUCTURES IN TRANSVERSE AND LONGITUDINAL PHASE SPACES*

C. -Y. Tsai#, Department of Physics, Virginia Tech, VA 24061, USA
R. Li, Jefferson Lab, Newport News, VA 23606, USA

Abstract

Microbunching instability (MBI) has been a challenging issue in high-brightness electron beam transport for modern accelerators. Our Vlasov analysis of MBI is based on single-pass configuration [1-3]. For multi-pass recirculation or a long beamline, the intuitive argument of quantifying MBI, by successive multiplication of MBI gains of sub-beamline sections, was found to underestimate the effect [4]. More thorough analyses based on concatenation of gain matrices aimed to combine both density and energy modulations for a general beamline [4]. Yet, quantification still focuses on characterizing longitudinal phase space; microbunching structures residing in (x,z) or (x',z) was observed in particle tracking simulation. Inclusion of such cross-plane microbunching structures in Vlasov analysis shall be a crucial step to systematically characterize MBI for a beamline complex in terms of concatenating individual beamline segments. We derived a semi-analytical formulation to include the microbunching structures in longitudinal and transverse phase spaces. Using these generalized formulas, we studied an example lattice [5] and found the microbunching gains calculated from multiplication of concatenated gain matrices can be considered as upper limit to the start-to-end gains.

INTRODUCTION

Theoretical formulation of MBI has been developed both in single-pass [1-3] and in storage-ring [6, 7] systems. Hetfeis *et al*. [2] derived a linear integral equation in terms of the density modulation (or, the bunching factor). Huang and Kim [3] obtained the integral equation in a more concise way and outlined the microbunching due to initial energy modulation. This has become the building block for our work.

To quantify MBI in a beam transport system, we estimate the microbunching amplification factor (or, gain) along the beamline. For a long transport line of a recirculation machine, people tend to treat the microbunching problem as a single-pass system. More commonly, concatenations of sub-beamline sections were studied and the overall microbunching gain is speculated as the multiplication of gains from individual subsections [2, 8]. Though this concatenation approach seems intuitive, we need a more rigorous and detailed justification of its validity. Our previous work [4], which takes both density (z) and energy (z, δ) modulations in longitudinal beam phase-space distribution, had shown that a mere product of microbunching gains from individual subsections could underestimate the overall effect (i.e. smaller than the start-to-end gain).

In this paper, we take a further step, consider the situation where microbunching structures residing in transverse-longitudinal dimension (x, z) or (x', z) can be quantified, and derive a set of governing equations for the microbunching evolution in terms of density, energy, transverse-longitudinal modulations along a general linear lattice. Then we study an example of recirculating beamline [5]. From the simulation results, we have some interesting observations and have found such combined analysis can give more information than the previous treatment. Although the formulation still appears incomplete, the gains calculated from multiplication of concatenated gain matrices can be considered as upper limit to the start-to-end gains. Comparison of the results with ELEGANT tracking [9] has given qualitative agreement. Extension of this study to include more aspects of microbunching can be possible future work.

THEORY

From the (linearized) Vlasov equation, the evolution of the phase-space distribution function is governed by [3]

$$f(X;s) = f_0(X_0) - \int_0^s d\tau \frac{\partial f_0(X_\tau)}{\partial \delta_\tau} \frac{d\delta}{d\tau} \tag{1}$$

where the energy change due to collective effect can be induced by density modulation

$$\frac{d\delta}{d\tau} = -\frac{Nr_e}{\gamma} \int \frac{dk_1}{2\pi} Z(k_1;\tau) b(k_1;\tau) e^{ik_1 z_\tau} \tag{2}$$

Here f is the beam phase-space distribution function, $X(s) = (x, x', z, \delta; s)$ the 4-D phase-space variable, N the number of particles, γ the Lorentz factor, $Z(k)$ the longitudinal impedance per unit length, k the modulation wavenumber, and $b(k)$ the density modulation.

More specifically, let us define the following quantities for subsequent analysis.

$$b(k_z;s) = \frac{1}{N} \int dX\, f(X;s) e^{-ik_z(s) z_s} \tag{3}$$

$$p(k_z;s) = \frac{1}{N} \int dX\, \left(\delta_s - h z_s\right) f(X;s) e^{-ik_z(s) z_s} \tag{4}$$

$$a_x(k_z;s) = \frac{1}{N} \int dX\, \left(x_s\right) f(X;s) e^{-ik_z(s) z_s} \tag{5}$$

$$a_{x'}(k_z;s) = \frac{1}{N} \int dX\, \left(x_s'\right) f(X;s) e^{-ik_z(s) z_s} \tag{6}$$

Figure 1 illustrates the modulations described by Eqs. (3-6), shown in (a) to (d), respectively.

* This material is based upon work supported by the U.S. Department of Energy, Office of Science, Office of Nuclear Physics under contract DE-AC05-06OR23177.
#jcytsai@vt.edu

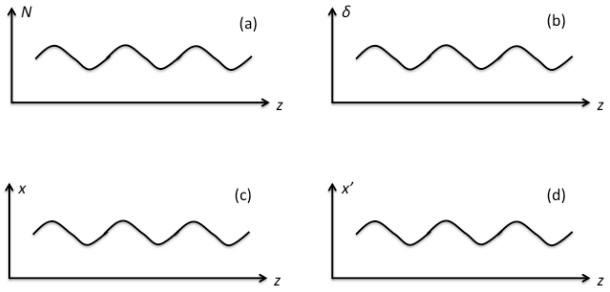

Figure 1: Illustration of various types of modulations.

Below we would consider how these different phase-space modulations evolve according to Eq. (1). The detailed derivation is not shown here and only the resultant formulas are summarized. The four integral equations governing $b(k_z)$, $p(k_z)$, $a_x(k_z)$, and $a_{x'}(k_z)$ are, respectively

$$b(k_z;s) = b_0(k_z;s) + \int_0^s d\tau K(\tau,s) b(k_z;\tau) \tag{7}$$

$$p(k_z;s) = p_0(k_z;s) + \int_0^s d\tau M(\tau,s) b(k_z;\tau) \tag{8}$$

$$a_x(k_z;s) = a_{x0}(k_z;s) + \int_0^s d\tau A(\tau,s) b(k_z;\tau) \tag{9}$$

$$a_{x'}(k_z;s) = a_{x'0}(k_z;s) + \int_0^s d\tau B(\tau,s) b(k_z;\tau) \tag{10}$$

where the kernel functions $K(\tau,s)$, $M(\tau,s)$, $A(\tau,s)$ and $B(\tau,s)$ describe the interaction (see Ref. [10] for complete expressions).

Of our particular interest, the beam phase-space distribution is assumed to be uniform in z and Gaussian over the remaining coordinates. The perturbed distribution function is assumed the following form

$$f_0(X_0) = \frac{n_0 + \Delta n_0(z_0)}{(2\pi)\varepsilon_{x0}\sqrt{2\pi}\sigma_\delta} e^{-\frac{(x_0+\Delta x_0(z_0))^2 + \left(\beta_{x0}(x_0'+\Delta x_0'(z_0)) + \alpha_{x0}(x_0+\Delta x_0(z_0))\right)^2}{2\varepsilon_{x0}\beta_{x0}} - \frac{(\delta_0 - hz_0 + \Delta\delta(z_0))^2}{2\sigma_\delta^2}} \tag{11}$$

where the individual perturbations are assumed to be small compared with the unperturbed one.

Note that there are a total of 4×4 =16 combinations for the above situations [see Eqs. (3-6) and (7-10)]. At each location, the modulations can be recorded as a *state vector*,

$$\mathbf{V}(s) \equiv \left[b(k_z;s)\ p(k_z;s)\ a_x(k_z;s)\ a_{x'}(k_z;s) \right]^T \tag{12}$$

$$b(k_z;s) = b^{(z)}(k_z;s) + b^{(\delta,z)}(k_z;s) + b^{(x,z)}(k_z;s) + b^{(x',z)}(k_z;s) \tag{13}$$

$$p(k_z;s) = p^{(z)}(k_z;s) + p^{(\delta,z)}(k_z;s) + p^{(x,z)}(k_z;s) + p^{(x',z)}(k_z;s) \tag{14}$$

$$a_x(k_z;s) = a_x^{(z)}(k_z;s) + a_x^{(\delta,z)}(k_z;s) + a_x^{(x,z)}(k_z;s) + a_x^{(x',z)}(k_z;s) \tag{15}$$

$$a_{x'}(k_z;s) = a_{x'}^{(z)}(k_z;s) + a_{x'}^{(\delta,z)}(k_z;s) + a_{x'}^{(x,z)}(k_z;s) + a_{x'}^{(x',z)}(k_z;s) \tag{16}$$

In the above expressions, the superscripts denote the modulations from either case illustrated in Fig. 1.

EXAMPLE

In this section, we would apply the generalized formulation to an example of recirculating machine [5]. This recirculating beamline consists of two arcs and the design is based on that outlined in Ref. [11]. One of the arcs is composed of 4 triple-bend-achromatic (TBA) units. The arcs are achromatic and quasi-isochronous. Let us separate this machine into four pieces: S1, ARC1, S2, and ARC2 (see Fig. 2). In this example, the beam is assumed 150 MeV in energy, peak bunch current 60 A, with normalized emittance 0.4 μm and relative energy spread 1.33×10^{-5}. Figure 3 shows Twiss and momentum compaction functions along the beamline.

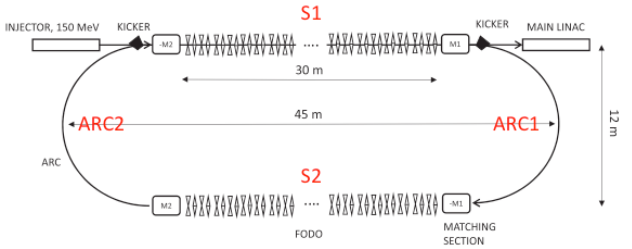

Figure 2: Schematic layout of the recirculating beamline (not to scale), from Ref. [5].

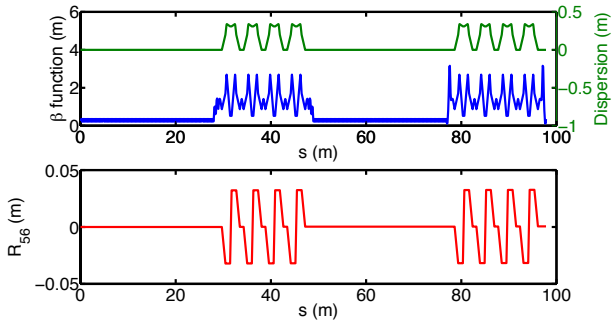

Figure 3: Twiss and momentum compaction functions along the beamline.

Below we would estimate both the density and energy modulations at the end of the beamline but begin from two different situations; one is start-to-end case [S1-ARC1-S2-ARC2] and the other is mid-to-end case [S2-ARC2]. Let us consider the following combinations:

(i) start-to-end case, with initial density modulation, $\mathbf{V}(0) = [1\ 0\ 0\ 0]^T$;

(ii) start-to-end case, with initial energy modulation, $\mathbf{V}(0) = [0\ 1\ 0\ 0]^T$;

(iii) mid-to-end case, the initial condition to S2 takes the value at the exit of ARC1, $\mathbf{V}(S2) = [b(k)\ p(k)\ a_x(k)\ a_{x'}(k)]^T$ for case (i) and (ii), based on the present 4-d theory;

(iv) mid-to-end case, the initial condition to S2 takes the value at the exit of ARC1, $\mathbf{V}(S2) = [b(k)\ p(k)\ a_x(k)\ a_{x'}(k)]^T$ for case (i) and (ii), based on 2-d theory [4].

The output state vectors are in general complex quantities. For example, for the resultant density modulation in Eq. (13), each individual contribution can have different phases. Taking absolute values for *all individual* contributions, the interference is then ignored and the resultant modulation can be considered as the

upper limit. This case is denoted as $G_\chi^{\sup} = \sum \left| \chi^{(\omega)} \right|$, where $\omega = (z),(\delta,z),(x,z),(x',z)$, and $\chi = b, p, a_x, a_{x'}$. For comparison, the other case with account of phase information is denoted as $G_\chi = \left| \sum \chi^{(\omega)} \right|$.

For simplicity, in what follows, we only include steady-state CSR [12,13], which only occurs in ARC1 and ARC2. For the case of initial density modulation, Fig. 4 shows the density and energy modulation spectra at the end of ARC2. From the figure, we can see differences between red and blue curves. The red curves, with output by taking absolute values for individual contributions, largely give the upper limit. The black curves can be considered as start-to-end gains for the beamline. The blue curves are found to underestimate the overall modulation. Similar results can be observed for the case of initial energy modulation, shown in Fig. 5.

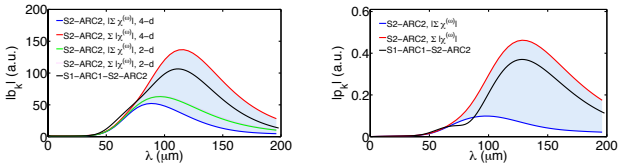

Figure 4: Density (left) and energy (right) modulation spectra with initial density modulation.

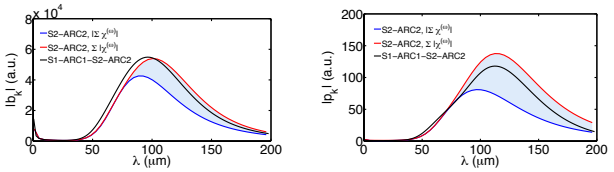

Figure 5: Density (left) and energy (right) modulation spectra with initial energy modulation.

In our previous work [4], we claimed that the underestimation of the 2-d $[b(k)\ p(k)]^T$ description originates from lack of inclusion of transverse-longitudinal correlations, e.g. (x,z) and/or (x',z) modulations, at ARC1 exit. Now we can estimate the modulation spectra residing in (x,z) and (x',z), shown in Fig. 6. To confirm, we used ELEGANT to track a large number (50-million) of particles and indeed observed the microbunching structures in (x, z) and (x', z), shown in Fig. 7.

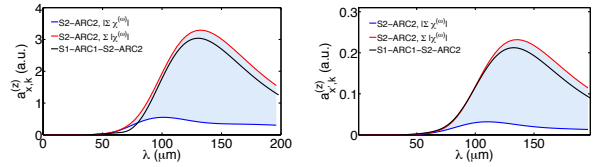

Figure 6: x-z (left) and x'-z (right) modulation spectra with initial density modulation.

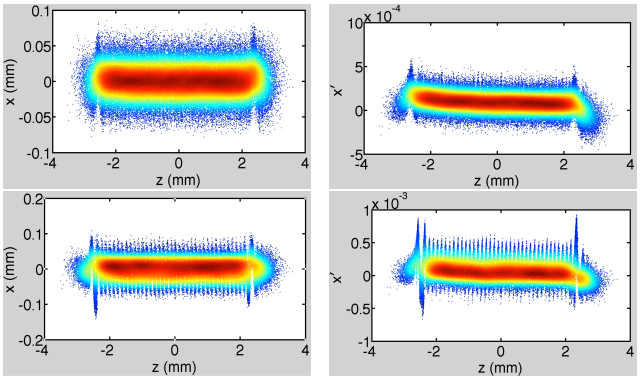

FIG. 7: Qualitative confirmation of transverse-longitudinal microbunching for λ = 50 μm (top) and λ = 125 μm (bottom) with initial density modulation.

To end this section, in the left figure of Fig. 4 we compare the microbunching gains calculated from three different ways: the start-to-end approach (black), the 4-d approach (red and blue curves, from S2 to ARC2) developed in this paper, and the 2-d approach (green curve and red dots, from S2 to ARC2) [4]. With inclusion of transverse-longitudinal microbunching structures, the calculated (concatenated) gains from sub-beamline section span a range, which largely covers the start-to-end gains. Figure 8 below shows the difference between the start-to-end results (black) and that obtained from intuitively direct multiplication of individual gains (blue).

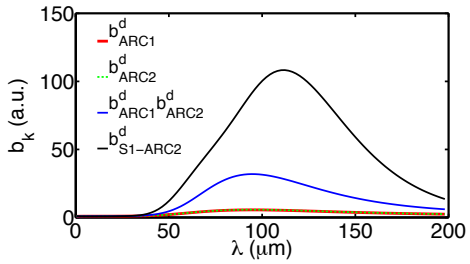

Figure 8: Comparison of density modulation spectra via start-to-end (black curve) and direct-multiplication (blue) consideration.

SUMMARY

In this paper we have derived a set of governing equations for microbunching in different dimensions, including density, energy, and transverse-longitudinal modulations, and apply to an example of recirculating machine. The Vlasov solutions and tracking simulations agree qualitatively with each other. Although the Vlasov results from concatenated sub-beamline sections do not match well with those obtained directly from the start-to-end results, $G^{sup} = \sum \left| \chi^{(\omega)} \right|$ gives upper limit for both density and energy modulations. In addition, the extended formulations can give us further insights on how upstream beamline sections can accumulate density, energy, and/or transverse-longitudinal microbunching, when the full-ring lattice is not provided.

REFERENCES

[1] See, for example, S. Heifets *et al*., Phys. Rev. ST Accel. Beams **5**, 064401 (2002)

[2] Z. Huang and K. Kim, Phys. Rev. ST Accel. Beams **5**, 074401 (2002)

[3] M. Vneturini, Phys. Rev. ST Accel. Beams **10**, 104401 (2007)

[4] C. -Y. Tsai and R. Li, IPAC'16 (TUPOR020)

[5] S. Di Mitri, Phys. Rev. ST Accel. Beams **17**, 074401 (2014)

[6] G. Stupakov and S. Heifets, Beam instability and microbunching due to coherent synchrotron radiation, Phys. Rev. ST Accel. Beams 5, 054402 (2002)

[7] See, for example, Y. Cai, Linear theory of microwave instability in electron storage rings, Phys. Rev. ST Accel. Beams 14, 061002 (2011)

[8] Z. Huang et al., Theory and simulation of CSR microbunching in bunch compressors, SLAC-PUB- 9538 (2002)

[9] M. Borland, elegant: A Flexible SDDS-Compliant Code for Accelerator Simulation, APS Report No. LS-287, 2000

[10] C. -Y. Tsai and R. Li, JLAB-TN-16-031

[11] D. Douglas *et al*., Control of coherent synchrotron radiation and microbunching effects during transport of high brightness electron beams, arXiv: 1403.2318v1 [physics.acc-ph]

[12] Y.S. Derbenev *et al*., Microbunch Radiative Tail-head Interaction, TESLA-FEL 95-05, 1995

[13] J. Murphy *et al*., Longitudinal wakefield for an electron moving on a circular orbit, Part. Accel. 1997, Vol. 57, pp. 9-64